

Diffusion is All You Need for Learning on Surfaces

Nicholas Sharp¹ Souhaib Attaki²
¹Carnegie Mellon University

Keenan Crane¹ Maks Ovsjanikov²
²LIX, École Polytechnique

Abstract

We introduce a new approach to deep learning on 3D surfaces such as meshes or point clouds. Our key insight is that a simple learned diffusion layer can spatially share data in a principled manner, replacing operations like convolution and pooling which are complicated and expensive on surfaces. The only other ingredients in our network are a spatial gradient operation, which uses dot-products of derivatives to encode tangent-invariant filters, and a multi-layer perceptron applied independently at each point. The resulting architecture, which we call DIFFUSIONNET, is remarkably simple, efficient, and scalable. Continuously optimizing for spatial support avoids the need to pick neighborhood sizes or filter widths a priori, or worry about their impact on network size/training time. Furthermore, the principled, geometric nature of these networks makes them agnostic to the underlying representation and insensitive to discretization. In practice, this means significant robustness to mesh sampling, and even the ability to train on a mesh and evaluate on a point cloud. Our experiments demonstrate that these networks achieve state-of-the-art results for a variety of tasks on both meshes and point clouds, including surface classification, segmentation, and non-rigid correspondence.

1. Introduction

In recent years there has been significant interest in applying learning techniques on non-uniform geometric data such as triangle meshes and 3D point clouds, inspired in part by the tremendous success of convolutional neural networks (CNNs) in computer vision applications. Due to the lack of regular grid structure enjoyed by images, basic building blocks of CNNs such as convolution and pooling are non-trivial to define on surfaces. A wide variety of approaches has emerged, proposing alternative constructions across different shape representations, e.g., [74, 64, 52, 28, 86], among many others.

A particularly important setting is applying learning techniques to surfaces represented as either triangle meshes or point clouds, representations common in applications from

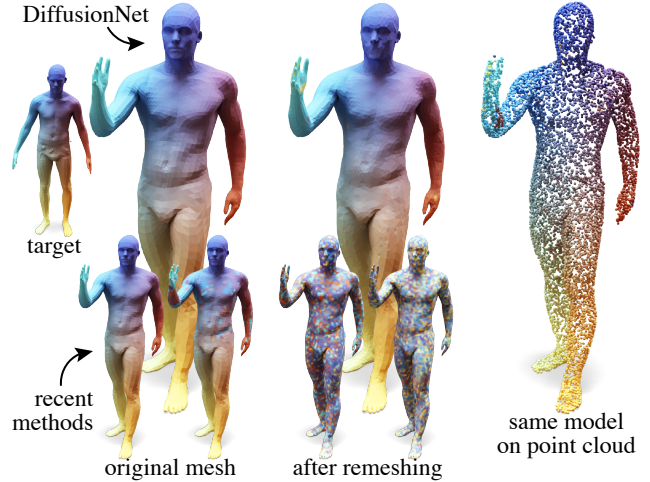


Figure 1. We propose learned diffusion as a powerful building block for deep learning on surfaces. Here, learned shape correspondences are visualized by the pullback of a color texture; alternate approaches [41, 20] produce excellent results on the dataset meshes (first column), but degrade dramatically after remeshing (middle column). DiffusionNet learns an accurate representation-agnostic solution, which even supports training on meshes and evaluating on a point cloud (last column).

robotics to computer graphics. Most successful learning methods are tied to a particular representation: point-based methods [64, 84, 77] are often simple and robust, but generally cannot leverage the underlying surface structure of the data. Conversely, mesh-based methods [52, 8, 62, 86] take advantage of the continuous surface structure, but often involve delicate geometric operations such as parallel transport, making them slow to train, difficult to replicate and not robust to changes in mesh sampling.

The gap between simple and robust point-based methods vs. accurate but complex and unstable mesh-based approaches presents an opportunity for innovation—principled geometric operations based on *discrete differential geometry* [54, 14] have been designed specifically to be robust to discretization. Chief among these techniques is the solution to standard partial differential equations, including the classic diffusion equation, for which reliable and efficient numer-

ical techniques have been developed on a range of shape representations [17, 45, 71].

In this paper we show that a state-of-the-art learning method on surfaces can be developed using only basic geometric tools: namely, simulating diffusion and computing spatial gradients. Specifically, we present DiffusionNet, an architecture for learning on surfaces that is both simpler and significantly more robust than previous surface-based techniques. More fundamentally, DiffusionNet offers a unified perspective across representations of surface geometry—in principle it can be applied to any geometric representation where one has a Laplacian and gradient operator (triangle meshes, point clouds, voxelizations, *etc.*). In this paper, for instance, we show how the same architecture achieves accurate results for both meshes and point clouds, and even allows training on one and evaluating on the other. We demonstrate through extensive experiments that our method achieves state-of-the-art accuracy and enables several novel applications in geometric deep learning.

Contributions. The main contributions of this work are:

- We show that a simple *learned* diffusion operation is sufficient to share spatial data in surface learning.
- We demonstrate that a spatial gradient layer can capture local directional information to learn invariant filters.
- Inspired by these insights, we present DiffusionNet, an architecture for learning on surfaces which has many advantages compared to past approaches, and achieves state-of-the-art results on several benchmarks.

2. Related Work

Applying deep learning techniques to 3D shapes is a rich and extensive area of research. Below we review the approaches most closely related to ours, and refer the interested readers to recent surveys, including [88, 9, 12].

View-based and volumetric methods. Most early geometric deep learning-based methods directly leveraged tools developed for 2D images, and thus mapped 3D shapes onto the plane either using multi-view renderings [74, 85, 33] or more global, often parametrization-based techniques such as panoramas [72, 69], geometry images [73], or metric-preserving mappings [19], among many others.

Another direct approach to applying convolution to 3D shapes relies on volumetric voxel grid representations, which has led to a variety of methods, including [87, 53] and their efficient extensions [83, 34]. Unfortunately such techniques are both computationally expensive and difficult to apply to detailed deformable shapes.

Learning on Surfaces. More closely related to ours are methods that apply learning techniques on 3D surfaces directly. These typically fall into two major categories based either on point cloud or triangle mesh representations.

Point-based methods. A very successful set of methods for learning on 3D shapes represented as point clouds was pioneered by the PointNet [64] and PointNet++ [65] architectures, which have been extended in many recent works, including PointCNN [43], DGCNN [84], PCNN [4] and KPConv [77] to name a few (see also [26] for a recent survey). Moreover, recent efforts have also been made to incorporate invariance and equivariance of the networks with respect to various geometric transformations, e.g., [16, 63, 91, 92, 42, 29]. The major advantages of point-based methods are their simplicity, flexibility, applicability in a wide range of settings and robustness in the presence of noise and outliers. However, first, their overall accuracy can often be lower than that of methods that explicitly use surface (e.g., mesh) connectivity. Second, these methods are typically not well-suited for *deformable* (non-rigid) shape analysis, and require extremely large training sets and significant data augmentation to achieve good results, e.g., for non-rigid shape matching applications [25, 18]. We note that globally supported point-based networks were recently considered in [60]. In contrast our method naturally allows global support via learned diffusion.

Surface and graph-based methods. To address the limitations of point-based approaches, several methods have been proposed that operate directly on surfaces and thus can learn filters that are intrinsic and robust to complex non-rigid deformations. The earliest pioneering approaches in this direction generalize convolutions [52, 8, 56, 20], typically using local surface parameterization via the logarithmic map—the intrinsic nature of these approaches make them well-suited to non-rigid shape matching problems. Unfortunately local parameterizations are only defined up to rotation in the tangent plane, leading to several methods which address this issue through design of *equivariant* surface networks [62, 31, 86]. While based on well-founded geometric principles, these methods often require complex operations such as parallel transport making them expensive to train and typically not applicable to point clouds.

The surface (mesh) structure has also been exploited in graph-based approaches, including [28, 80, 46, 24] or even using Recurrent Neural Networks for defining random walks on meshes [36] among others. While accurate, these methods can be costly on densely sampled shapes and often are not robust to significant changes in the mesh structure.

Spectral methods. Our use of diffusion is also closely related to techniques that operate in the spectral domain and often exploit the link between convolution and operations in a derived (e.g., Fourier or Laplace-Beltrami) basis, including [15, 38, 76]. Such methods have a long history in graph-based learning and are well-rooted in machine learning and data analysis more broadly, with Laplacian eigenmaps [5], spectral clustering [79] and diffusion maps [13] as well-known closely related examples. In geometry processing, spectral methods have been used for a range of tasks including multi-resolution representation [39], segmentation [68] and matching [58] among others [79, 90].

Unfortunately, Laplacian eigenfunctions depend on each shape and thus coefficients or learned filters from one shape are not trivially transferable to another. Functional maps [58] can be used to “translate” coefficients between shapes, and have been used, e.g., in [89] jointly with spectral filter learning. More recently deep functional maps [48] have been proposed to learn optimal features for correspondences with functional maps, and have been extended in follow-up works, e.g., [18]. However, the features are still learned either with MLPs starting from pre-computed descriptors [48, 67, 22] or using point-based architectures [18].

Instead, we propose an approach that learns the parameters of the physical diffusion process that are directly transferable across training and test shapes and, as we show below, can be used effectively in non-rigid shape matching applications.

We also remark that our use of the Laplacian in defining the diffusion operator is similar to the Surface networks [35], CayleyNets [38] and their recent application in shape matching using ChebyshevNets [41]. However, we demonstrate that complex polynomial filters can be replaced with simple diffusion, and moreover that local functional gradients can be used to inject orientation information into the network, leading to improved performance and robustness.

The use of diffusion was also suggested in [29], although that work proposes to learn linear combinations of pre-defined diffusion kernels. In contrast, our method directly learns a diffusion time per-feature, incorporates a learned gradient operation, and is applied directly to mesh surfaces.

Pooling Finally, we remark that in 3D learning it is non-trivial to define pooling, especially on meshes where it often amounts to mesh simplification [28]. Various recent operations have been proposed for point cloud [47, 32], mesh [55, 93] or even graph pooling [49, 40]. A key advantage of our approach is that it automatically optimizes for spatial support without any many pooling or U-Net architecture, greatly simplifying implementation and improving learning.

3. Method

Our method consists of three main building blocks: point-wise multi-layer perceptrons (MLPs) for aggregating information across different channels, applied independently at every point, learned diffusion for propagating information across points and local gradients for extracting local changes (variability) in the signal. We first describe our main numerical components, and then we assemble them into an effective architecture in Section 4. Our method is defined in a representation-agnostic manner; applying it to meshes or point clouds simply amounts to assembling the appropriate Laplacian and gradient matrices as we discuss below.

3.1. Pointwise Perceptrons

On a mesh or point cloud with V vertices, we consider a collection of C scalar features defined at each vertex. Our first basic building block is a pointwise function $f : \mathbb{R}^C \rightarrow \mathbb{R}^C$, which is applied identically at every vertex to transform the features. We represent these pointwise functions as a standard multilayer perceptron (MLP) with shared weights across all vertices. Although these MLPs can fit arbitrary functions at each point, they do not capture the *spatial structure* of the surface, or even allow any communication between vertices, so a richer structure is needed.

Past approaches have ranged from global reductions to explicit geodesic convolutions—instead, we will demonstrate that a simple *learned* diffusion layer can help propagate information efficiently, and with greater control over locality.

3.2. Learned Diffusion

In the continuous setting, diffusion of any quantity x is modeled by the *heat equation*

$$\frac{d}{dt}x(t) = \Delta x(t), \quad (1)$$

where Δ is the Laplacian (or more formally: the *Laplace-Beltrami operator*). The longer we diffuse, the more global communication becomes: for $t = 0$ we just have the identity map, and as $t \rightarrow \infty$, the diffused quantity approaches its average over the whole surface.

We propose to use the heat equation to spatially propagate features in our network; its principled foundations ensure that results are largely invariant to the way the surface is sampled or meshed. To discretize it, one replaces Δ with a negative semi-definite matrix $L \in \mathbb{R}^{V \times V}$. This matrix has been defined for voxel grids [11], polygon meshes [10], tetrahedral meshes [2], *etc.* For triangle meshes, the *cotan-Laplace* matrix is ubiquitous in geometry processing applications [50, 61, 14]; in our implementation, we use the robust cotan-Laplacian as well as the related point cloud Laplacian from [71].

Our learned diffusion layer $h : \mathbb{R}^{V \times C} \rightarrow \mathbb{R}^{V \times C}$ independently diffuses each channel x_i for a learned time $t_i \in \mathbb{R}_{\geq 0}^C$.

Each scalar feature $x_i \in \mathbb{R}^V$ can be diffused by computing $x_i(t) = \exp(t_i L)x_i(0)$, where $\exp : \mathbb{R}^{V \times V} \rightarrow \mathbb{R}^{V \times V}$ is the matrix exponential. In practice, we do not directly evaluate this exponential, but rather use the reduced spectral basis for efficiency (Sec. 3.3). Learning the diffusion parameter is a key strength of our method, allowing the network to continuously optimize for the spatial support ranging from purely local to totally global, and even choose different receptive fields for each feature. We thus sidestep challenges like manually choosing the support radius of a convolution, or sizes for a pooling hierarchy.

A note on generality. Remarkably, eschewing traditional representations of convolutions in favor of diffusion does not reduce the expressive power of our networks. This is supported by the following theoretical result (that we prove in the supplement):

Lemma 1 *There exists a pointwise function that maps the diffused values $x_p(t)$ at a fixed point p for all $t > 0$ to the value of a radially-symmetric convolution against $x(0)$ at p .*

This fact is significant because it suggests that simple and robust diffusion can, without loss of generality, be used to replace complex operations such as geodesic convolution. Importantly, we will also extend our architecture to a broader space beyond radially-symmetric convolutions by incorporating gradient features (Sec. 3.4).

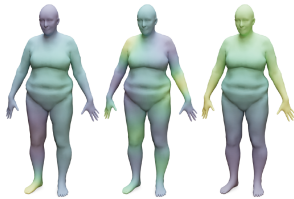
3.3. Spectral Evaluation

In principle, any numerical scheme could be used to simulate diffusion—we choose to work in a basis of low-frequency Laplacian eigenfunctions [79, 90] since (i) diffusion quickly damps high-frequencies, and (ii) working in such a basis reduces computation to dense arithmetic. In particular, for any Laplace and mass matrices $L, M \in \mathbb{R}^{V \times V}$, *resp.*, we consider the solutions $\phi_i \in \mathbb{R}^V$ to

$$L\phi_i = \lambda_i M\phi_i, \quad (2)$$

for the first k smallest-magnitude eigenvalues $\lambda_1, \dots, \lambda_k$. These bases are easily precomputed for each shape of interest via standard numerical packages [37]; the inset shows several example functions ϕ_i .

Let $U := [\phi_i] \in \mathbb{R}^{V \times k}$ be the stacked matrix of eigenvectors, which form an orthonormal basis with respect to M . We can then project any scalar function x to obtain its coefficients c in the spectral basis via $c \leftarrow U^T Mx$, and recover values at vertices as $x \leftarrow Uc$.



Spectral diffusion. Conveniently, diffusion for time t is easily expressed as an elementwise operation on spectral coefficients

$$c_{i,t} = e^{-\lambda_i t} c_{i,0}. \quad (3)$$

Our learned diffusion layer is then evaluated by projecting on to the spectral basis, evaluating pointwise diffusion, and projecting back

$$h(x) := U \begin{bmatrix} e^{-\lambda_0 t_0} \\ e^{-\lambda_1 t_1} \\ \dots \end{bmatrix} \odot (U^T Mx) \quad (4)$$

where \odot denotes the Hadamard (element-wise) product. This operation is trivially differentiable with respect to learned t_i , and easily evaluated using dense linear algebra.

Notice that in contrast to typical spectral filtering [15], we do not learn frequency-specific filters; we merely leverage the spectral basis as a computational scheme to evaluate diffusion. For this reason, our method does not suffer from differing eigenbases on different shapes—a common challenge in past approaches.

3.4. Spatial Gradient Operations

Our learned diffusion layer enables propagation of information across different points on the shape, but it allows only radially-symmetric filters about a point. The last building block in our pipeline enables a larger space of filters by computing additional features from the spatial gradients of signal values at vertices. Specifically, we construct features from the inner products between pairs of gradients at each vertex, after applying a learned rotation.

Evaluating gradients. The spatial gradient of a scalar function on a surface is a 2D vector defined in the tangent space of each vertex. These gradients can be evaluated by a standard procedure, choosing a normal vector at each vertex (given as input or locally approximated), then projecting neighbors into the tangent plane—either 1-ring neighbors on a mesh, or k -nearest neighbors in a point cloud. Gradients are then computed via a linear least-squares approximation of the function values [57]. The global gradient operator can then be represented as a (sparse) matrix $G \in \mathbb{C}^{V \times V}$, which is applied to real values at vertices to produce gradient tangent vectors at each vertex. Here, complex numbers are merely a notational convenience for 2D tangent vectors.

Rather than directly applying G to evaluate gradients in our network, we compose G with the spectral basis U as $\tilde{G} := GU$ to form the dense matrix $\tilde{G} \in \mathbb{C}^{V \times k}$ which maps spectral coefficients to gradient vectors at each vertex. We then apply \tilde{G} to the spectral feature coefficients already available from the diffusion. This strategy has two benefits: it avoids sparse matrix operations at evaluation time in favor of dense arithmetic, and stabilizes repeated gradient operations by effectively truncating high-frequency components.

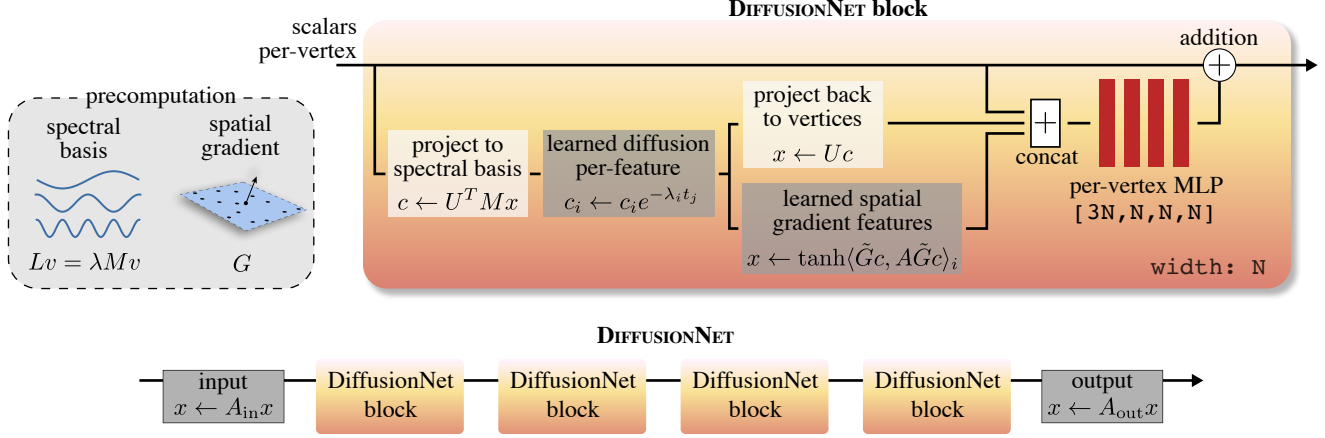


Figure 2. We present DiffusionNet, a simple and effective architecture for learning on surfaces. It is composed of successive identical DiffusionNet Blocks, each of which diffuses each feature for a learned time scale, forms spatial gradient features, and applies a pointwise MLP at each vertex. These networks achieve state of the art performance on surface learning tasks without any explicit convolution, pooling, or normalization layers, in part because they can automatically optimize for variable spatial support.

Learned pairwise products. Equipped with per-vertex spatial gradients of each channel, we learn informative scalar features by evaluating a dot-product between pairs of feature gradients at each vertex. Dot products are invariant to rotations of the coordinate system, so these features are independent to the choice of vertex tangent spaces, as expected. In particular, given tangent vectors $z \in \mathbb{C}^C$ at a vertex, we form the features $h \in \mathbb{R}^C$ as

$$h_i := \tanh(\langle z, Az \rangle_i) \quad (5)$$

where A is a learned square $C \times C$ matrix, and $\langle \cdot, \cdot \rangle_i$ denotes the element-wise dot product of the each pair of vectors. The outer $\tanh(\cdot)$ nonlinearity is not fundamental, but we find that remapping the activations to $[-1, 1]$ stabilizes training.

The choice of A as a complex or real matrix has a subtle relationship with the orientation of the underlying surface. Complex A models a linear combination of tangent vectors after scaling *and rotating* each vector, whereas real A only allows scaling. In particular, surfaces with consistently oriented normals gain a richer representation by learning a complex matrix, whereas surfaces without consistent orientation (such as raw point clouds) must learn a real A which cannot rotate vectors. We provide an extended discussion of this property in the supplement, and show how the expressive power of orientation allows our network to disambiguate bilateral symmetry even in an intrinsic formulation.

4. DiffusionNet Architecture and Training

The previous section established three simple core ingredients for learning on surfaces: pointwise functions at each vertex approximated as MLPs, learned diffusion for spatial communication, and spatial gradients for local variability

estimation. We combine these ingredients to construct *DiffusionNet* (Fig. 2), composed of several *DiffusionNet blocks*. This simple network operates on a fixed channel width C of scalar values throughout, with each DiffusionNet block diffusing the features, constructing gradient dot-product features, and feeding the result to an MLP.

We include residual connections to stabilize training [30], as well as linear layers at the beginning and end of the network to convert to the expected input and output dimension. Various activations can be appended to the end of the network based on the problem at hand, such as a softmax for classification; otherwise, this same architecture is used for all experiments. Remarkably, we do not find it necessary use any pooling or normalization—a major reason for the generality and robustness of our networks.

Invariance. We remark that our architecture is fully invariant to rigid motion of the underlying shapes, assuming that the input features remain unchanged. This invariance is due to the intrinsic geometric nature of diffusion and spatial gradient operations. This means that the overall invariance of the network can be controlled through the choice of input features, as discussed below.

4.1. Input features

Our networks can easily use any kind of scalar data as input features. In our experiments, we use either raw 3D coordinates as input or Heat Kernel Signatures (HKS)[75], as appropriate for the problem. Higher-order descriptors such as SHOT [78] seem to be unnecessary due to the expressive power of our architecture. We also avoid these as recent works [18] have shown significant instability of such descriptors under changes in mesh structure.

Method	Accuracy
GWCNN [19]	90.3%
MeshCNN [28]	91.0%
HSN [86]	96.1%
DiffusionNet - hks (ours)	98.0%
DiffusionNet - xyz (ours)	98.9%

Table 1. Results from mesh classification on 30-class SHREC11 [44], training on just 10 samples per class. Additional comparisons achieving $< 90\%$ accuracy can be found in [19, 86].

Coordinates. In settings where the initial rigid orientation of an input shape is semantically meaningful we use the raw 3D coordinates of the shapes as input features. We also can apply data augmentation to learn invariance in settings where shapes are expected not to be consistently oriented.

Heat kernel signatures. In settings where rigid or even non-rigid invariance is desired, such as non-rigid shape correspondence problems, we use Heat Kernel Signatures [75] as input to our network; these signatures are trivially computed from the spectral basis in Sec. 3.3. Due to the intrinsic and fully geometric nature of our approach, with HKS as input, our resulting networks are fully invariant to orientation-preserving isometric deformations of the shape.

4.2. Subsampling

As mentioned above, our approach is naturally robust to changes in sampling and discretization due to its geometric nature. In extreme cases, where robustness is required due to significant changes in sampling density, we propose an additional simple and efficient strategy, consisting of randomly sub-sampling shapes during training. We do not use this strategy in any of our experiments, but we describe it in the supplement as a potentially useful variant of our approach.

5. Experiments and Analysis

Due to the simplicity, efficiency, and generality of our approach, we can easily evaluate it on a wide variety of challenging tasks in geometric learning. The same network architecture—without any explicit pooling or convolutions—achieves state-of-the-art results for learning problems on both meshes and point clouds. The supplement includes extended results and analysis of our method, such as an ablation study and a parameter sweep over the size of the truncated spectral basis.

Setup. Our experiments use a small 32-width (30k parameter) or large 128-width (0.5M parameter) 4-block DiffusionNet, depending on the scale of the problem. The pointwise MLPs use ReLU activations after all linear layers except the last, optionally followed by dropout with $p = 0.5$. The network ends with a final softmax for classification and

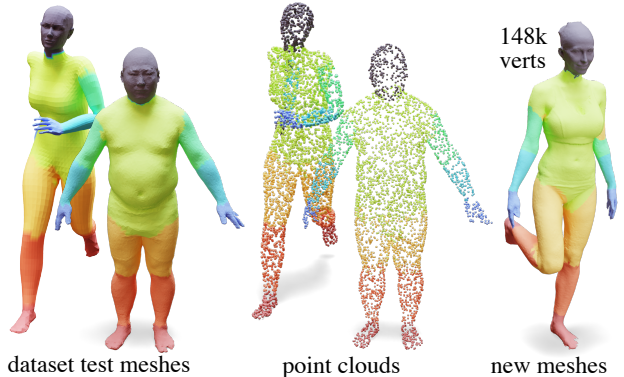


Figure 3. After training to segment the mesh dataset of [51] (*left*), our model yields accurate results on point clouds sampled from the same dataset (*middle*), as well as shapes from totally different sources (*right*): a large raw scan mesh from FAUST [7].

segmentation tasks. We fit the model using the ADAM optimizer with an initial learning rate of 0.001 and a batch size of 1, training for 200 epochs and decaying the learning rate by a factor of 0.5 every 50 epochs. Spectral computation is truncated to a $k = 128$ eigenbasis, and we use 30 neighbors to build point clouds gradient matrices. All inputs are centered and scaled to be contained in a unit sphere at the origin before processing, and HKS is sampled at 16 values of t logarithmically spaced between $t \in [0.01, 1]$ after scaling. Accuracies are reported at the conclusion of training.

Implementation details. Precomputation, such as computing the spectrum of the Laplacian, is performed once as a preprocess on the CPU using SciPy [81, 37]; networks are implemented in PyTorch [59]. Code will be made public after review. Performance is summarized in Sec. 5.5.

5.1. Classification

SHREC-11. We first apply our method to classify meshes in the SHREC-11 dataset [44] into 30 categories, using a 32-width DiffusionNet on this small problem. As in past work [19], we train on just 10 samples per class, and we report results averaged over 3 random samplings of the training data. Our network repeatedly achieves the highest reported classification accuracy (Tab. 1), perhaps due to its low parameter count (30k), and principled formulation.

5.2. Segmentation

Human segmentation. We train a 32-width DiffusionNet to segment the human body parts on the composite dataset of [51], containing models from several other human shape datasets [7, 3, 1, 82, 23]. Our model is quite effective using both raw coordinates with rotation augmentation and HKS as input, with the second-best reported accuracy among recent methods.

Method	Accuracy
MDGCNN [62]	88.6%
DGCNN [84]	89.7%
PointNet++ [64]	90.8%
SNGC [27]	91.0%
HSN [86]	91.1%
MeshCNN [28]	92.3%
DiffusionNet - hks	91.5%
DiffusionNet - xyz	90.9%

Table 2. Accuracy for human part segmentation on the dataset of [51]. Additional comparisons below 90% are found in [27].

	Method	Accuracy
point cloud	PCNN [4]	78.0%
	PointNet++ [64]	74.4%
	SPHNet [63]	80.1%
	DiffusionNet - xyz	85.0%
mesh	SplineCNN [20]	53.6%
	SurfaceNetworks [35]	88.5%
	DiffusionNet - xyz	90.3%
	DiffusionNet - hks	90.8%

Table 3. Accuracy of various mesh and point cloud schemes for RNA segmentation. DiffusionNet achieves state-of-the-art results, in part because it can be applied directly to the raw meshes.

Molecular segmentation. We evaluate a 128-width DiffusionNet on the task of segmenting RNA molecules into functional components, using the dataset introduced in [63]. This dataset consists of 640 RNA surface meshes of about 15k vertices each extracted from [6], labelled at each vertex according to 259 atomic categories. Our experiments use a random 80/20 train-test split. We learn these labels on point clouds of 4096 uniformly-sampled points on the shape as in [63], as well as learning directly on the raw meshes. For comparison, we cite point cloud results reported in [63], and additionally train SplineCNN [20] and a Dirac Surface Network [35] on meshes. We also attempted to train MeshCNN [28] and HSN [86], but found the former prohibitively expensive, while the latter struggled to successfully preprocess the data. Our method achieves state-of-the-art accuracy on both the mesh and point cloud variants of the problem (Tab. 3). Learning directly on the mesh yields greater accuracy, perhaps because no information is lost when sampling a point cloud and surface structure is preserved (Fig. 4).

5.3. Functional Correspondence

Functional maps indirectly compute a correspondence by finding a linear transformation between spectral bases on a pair of shapes, aligning some set of input features

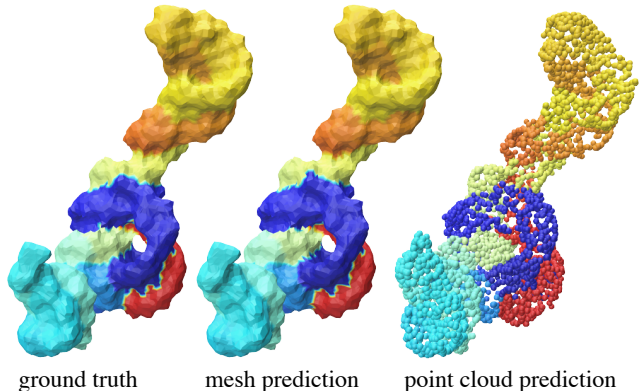


Figure 4. Segmenting RNA molecules with our method achieves accurate results when applied either directly to the raw meshes or to sampled point clouds.

Method / Dataset	FAUST	SCAPE	FonS	SonF
KPConv [18]	3.1	4.4	11.0	6.0
KPConv - hks [18]	2.90	3.28	10.65	5.55
HSN [86]	3.29	3.53	25.41	16.66
ACSCNN [41]	2.75	3.22	8.44	6.08
DiffusionNet - hks	2.53	2.97	5.61	3.00

Table 4. Our approach yields state-of-the-art correspondence results when used as a feature extractor for deep functional maps [18]. X on Y means train on X and test on Y. Reported error values are mean geodesic error $\times 100$ on shapes normalized to have unit area.

[58]. Recent work has shown that *learned features* can improve performance [48, 18] and lead to state-of-the-art point-to-point shape correspondences. We benchmark our approach against recent feature extractors for this task. Our experiments mimic the setup of [18], trained and evaluated on both FAUST [7] and SCAPE [3, 66] (including training on one dataset and evaluating on the other). To compare rigid-invariant models, we randomly rotate all inputs for testing and training; additional results on canonical orientations are provided in the supplement. In all cases we extract point-to-point maps between test shapes and evaluate them against ground truth dense correspondences. In addition to KPConv [77] as used in [18], we train MeshCNN [28], HSN [86], ACSCNN [41], and our DiffusionNet, keeping the same training loss as in [18]. MeshCNN proved to be prohibitively expensive, at 14hr per epoch.

As shown in Tab. 4 DiffusionNet yields state-of-the-art results for non-rigid shape correspondence, especially when transferring between datasets. One might wonder whether the improvement in this task stems from our HKS features, or truly from our DiffusionNet architecture—training KPConv with HKS as features shows DiffusionNet yields significant improvements regardless.

Method	orig	remeshed/sampled variants			
		iso	dense	qem	cloud
HSN	4.16	12.96	22.10	21.55	-
SplineCNN	2.24	32.10	26.46	42.17	-
ACSCNN	0.05	35.29	19.09	41.15	-
DiffusionNet	0.50	1.15	1.99	1.33	3.07

Table 5. Accuracy of vertex-labelling correspondence on our remeshed FAUST dataset. All methods are trained only on the original canonically-meshed training set. Errors are given in mean geodesic distance $\times 100$, after normalizing by the geodesic diameter.

5.4. Sampling Invariance

We further study the robustness of our network to mesh connectivity and sampling changes. For this, we consider a variant of the correspondence task on FAUST [7] where each vertex is to be labelled with the corresponding nearest vertex on a template mesh. Importantly, these input meshes are already aligned templates produced by a manual annotation process, with exactly isomorphic mesh connectivity among the training and test set. Past work has achieved near-perfect accuracy in this problem setup (e.g. [20, 41]), however we suggest that existing models primarily learn the mesh graph structure rather than a function of the shape itself.

To analyze this phenomenon, we construct a variant of the FAUST test set via several remeshing strategies: *orig* is the original mesh, *iso* is a uniform isotropic remeshing, *dense* refines the mesh in randomly sampled regions, *qem* first refines the meshes, then applies quadric error simplification [21], and *cloud* is a sampled point cloud with normals. (An unrelated remeshing appeared in [62, 86], but the procedure therein left large regions of the mesh unchanged.) We train models on the first 80 standard FAUST registered meshes, but evaluate on this remeshed set. This setting mimics a practical scenario, where training data contains sampling biases, yet the fitted model must be applied to different meshes encountered in the wild. In Table 5 we compare DiffusionNet to other recent surface learning algorithms. For fairness, all models are trained on the raw coordinates of the meshes. We see that the results of other algorithms degrade rapidly under remeshing; only DiffusionNet yields reasonable correspondence results on *any* altered mesh connectivity (Fig. 5).

5.5. Performance

DiffusionNet requires only dense arithmetic for training and inference, and is thus straightforward and efficient on modern hardware. On an RTX2070 GPU and i7-10700K CPU, training directly on the 15k-vertex RNA meshes from Sec. 5.2 takes about 42 milliseconds each. Our preprocessing assembles matrices and computes eigenvectors; preprocessing the 7k-vertex FAUST meshes takes about 2 seconds each.

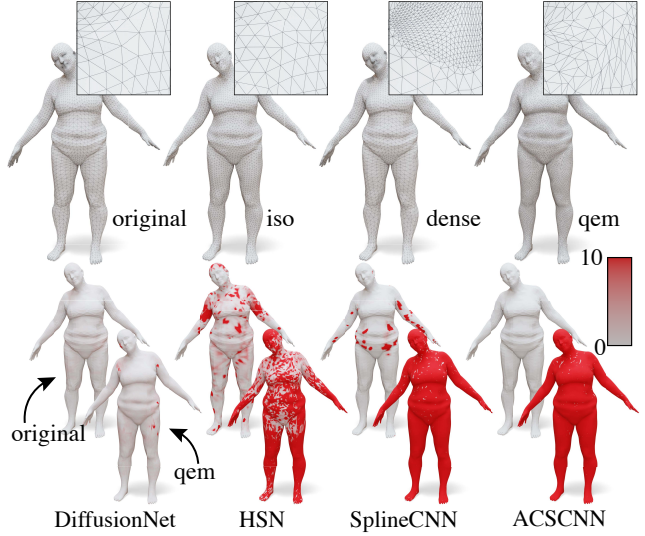


Figure 5. We investigate invariance to mesh sampling on top-performing correspondence algorithms. *Top*: the test set is remeshed according to three policies. *Bottom*: correspondence error evaluated on the original connectivity, and on the *qem* remeshed connectivity (as in Tab. 5). Only DiffusionNet remains remotely accurate after remeshing the input.

Memory usage is quite modest, which has the practical benefit of enabling our networks to run directly on large input meshes without resampling or simplification. The meshes from [51] have up to 13k vertices, yet recent approaches downsample to roughly 1k vertices [28, 86], while our networks easily run at full resolution with just 2.5GB memory usage, training at 8 seconds/epoch.

Our method offers significant practical benefits with its scalability, particularly at inference time: we evaluate on a raw scan mesh with 148k vertices in Fig. 3, no special treatment is needed, preprocessing takes 43 sec, and model evaluation takes 150ms with 2.7GB GPU memory usage.

6. Conclusion, Limitations, and Future Work

We present a novel approach for learning on surfaces that achieves state-of-the-art results using only simple principled geometric operations: learned diffusion and spatial gradients. Our method is very efficient to train and evaluate, is robust to changes in sampling, and even generalizes across representations, without relying on any hierarchies or pooling.

Although our method discourages overfitting to mesh sampling (Sec. 5.4), it cannot guarantee to eliminate it, and we still observe a drop in performance when transferring between representations—further investigation may develop additional regularization schemes. In the future, it is promising to study our approach in other settings, such as learning on graphs or implicit level sets, offering a unified domain-agnostic surface learning framework.

References

- [1] Adobe. Adobe mixamo 3d characters, 2016. www.mixamo.com. 6
- [2] Marc Alexa, Philipp Herholz, Maximilian Kohlbrenner, and Olga Sorkine-Hornung. Properties of laplace operators for tetrahedral meshes. In *Computer Graphics Forum*, volume 39, pages 55–68. Wiley Online Library, 2020. 3
- [3] Dragomir Anguelov, Praveen Srinivasan, Daphne Koller, Sebastian Thrun, Jim Rodgers, and James Davis. Scape: shape completion and animation of people. In *ACM SIGGRAPH 2005 Papers*, pages 408–416. 2005. 6, 7
- [4] Matan Atzmon, Haggai Maron, and Yaron Lipman. Point convolutional neural networks by extension operators. *ACM Transactions on Graphics (TOG)*, 37(4):1–12, 2018. 2, 7
- [5] Mikhail Belkin and Partha Niyogi. Laplacian eigenmaps for dimensionality reduction and data representation. *Neural computation*, 15(6):1373–1396, 2003. 3
- [6] Helen M Berman, John Westbrook, Zukang Feng, Gary Gilliland, Talapady N Bhat, Helge Weissig, Ilya N Shindyalov, and Philip E Bourne. The protein data bank. *Nucleic acids research*, 28(1):235–242, 2000. 7
- [7] Federica Bogo, Javier Romero, Matthew Loper, and Michael J Black. Faust: Dataset and evaluation for 3d mesh registration. In *Proceedings of the IEEE Conference on Computer Vision and Pattern Recognition*, pages 3794–3801, 2014. 6, 7, 8, 14
- [8] Davide Boscaini, Jonathan Masci, Emanuele Rodolà, and Michael Bronstein. Learning shape correspondence with anisotropic convolutional neural networks. In *Advances in neural information processing systems*, pages 3189–3197, 2016. 1, 2
- [9] Michael M Bronstein, Joan Bruna, Yann LeCun, Arthur Szlam, and Pierre Vandergheynst. Geometric deep learning: going beyond euclidean data. *IEEE Signal Processing Magazine*, 34(4):18–42, 2017. 2
- [10] Astrid Bunge, Philipp Herholz, Misha Kazhdan, and Mario Botsch. Polygon laplacian made simple. In *Computer Graphics Forum*, volume 39, pages 303–313. Wiley Online Library, 2020. 3
- [11] Thomas Caissard, David Coeurjolly, Jacques-Olivier Lachaud, and Tristan Roussillon. Laplace–beltrami operator on digital surfaces. *Journal of Mathematical Imaging and Vision*, 61(3):359–379, 2019. 3
- [12] Wenming Cao, Zhiyue Yan, Zhiqian He, and Zhihai He. A comprehensive survey on geometric deep learning. *IEEE Access*, 8:35929–35949, 2020. 2
- [13] Ronald R Coifman, Stephane Lafon, Ann B Lee, Mauro Maggioni, Boaz Nadler, Frederick Warner, and Steven W Zucker. Geometric diffusions as a tool for harmonic analysis and structure definition of data: Diffusion maps. *Proceedings of the national academy of sciences*, 102(21):7426–7431, 2005. 3
- [14] Keenan Crane, Fernando De Goes, Mathieu Desbrun, and Peter Schröder. Digital Geometry Processing with Discrete Exterior Calculus. In *ACM SIGGRAPH Courses*, pages 1–126. 2013. 1, 3
- [15] Michaël Defferrard, Xavier Bresson, and Pierre Vandergheynst. Convolutional neural networks on graphs with fast localized spectral filtering. In *Advances in neural information processing systems*, pages 3844–3852, 2016. 3, 4
- [16] Haowen Deng, Tolga Birdal, and Slobodan Ilic. Ppf-foldnet: Unsupervised learning of rotation invariant 3d local descriptors. In *Proceedings of the European Conference on Computer Vision (ECCV)*, pages 602–618, 2018. 2
- [17] Mathieu Desbrun, Mark Meyer, Peter Schröder, and Alan H Barr. Implicit fairing of irregular meshes using diffusion and curvature flow. In *Proceedings of the 26th annual conference on Computer graphics and interactive techniques*, pages 317–324, 1999. 2
- [18] Nicolas Donati, Abhishek Sharma, and M. Ovsjanikov. Deep geometric functional maps: Robust feature learning for shape correspondence. *2020 IEEE/CVF Conference on Computer Vision and Pattern Recognition (CVPR)*, pages 8589–8598, 2020. 2, 3, 5, 7
- [19] Danielle Ezuz, Justin Solomon, Vladimir G Kim, and Mirela Ben-Chen. Gwcnn: A metric alignment layer for deep shape analysis. In *Computer Graphics Forum*, volume 36, pages 49–57. Wiley Online Library, 2017. 2, 6
- [20] Matthias Fey, Jan Eric Lenssen, Frank Weichert, and Heinrich Müller. Splinecnn: Fast geometric deep learning with continuous b-spline kernels. In *Proceedings of the IEEE Conference on Computer Vision and Pattern Recognition*, pages 869–877, 2018. 1, 2, 7, 8
- [21] Michael Garland and Paul S Heckbert. Surface simplification using quadric error metrics. In *Proceedings of the 24th annual conference on Computer graphics and interactive techniques*, pages 209–216, 1997. 8
- [22] Dvir Ginzburg and Dan Raviv. Cyclic functional mapping: Self-supervised correspondence between non-isometric deformable shapes. *Proc. ECCV*, 2020. 3
- [23] Daniéla Giorgi, Silvia Biasotti, and Laura Paraboschi. Watertight models track. In *Shape Retrieval Contest 2007: CNR—IMATI Via De Marini* 6, number 16149. 2007. 6
- [24] Shunwang Gong, Lei Chen, Michael Bronstein, and Stefanos Zafeiriou. Spiralnet++: A fast and highly efficient mesh convolution operator. In *Proceedings of the IEEE International Conference on Computer Vision Workshops*, pages 0–0, 2019. 2
- [25] Thibault Groueix, Matthew Fisher, Vladimir G. Kim, Bryan Russell, and Mathieu Aubry. 3d-coded : 3d correspondences by deep deformation. In *ECCV*, 2018. 2
- [26] Yulan Guo, Hanyun Wang, Qingyong Hu, Hao Liu, Li Liu, and Mohammed Bennamoun. Deep learning for 3d point clouds: A survey. *IEEE transactions on pattern analysis and machine intelligence*, 2020. 2
- [27] Niv Haim, Nimrod Segol, Heli Ben-Hamu, Haggai Maron, and Yaron Lipman. Surface networks via general covers. In *Proceedings of the IEEE International Conference on Computer Vision*, pages 632–641, 2019. 7
- [28] Rana Hanocka, Amir Hertz, Noa Fish, Raja Giryes, Shachar Fleishman, and Daniel Cohen-Or. Meshcnn: a network with an edge. *ACM Transactions on Graphics (TOG)*, 38(4):1–12, 2019. 1, 2, 3, 6, 7, 8
- [29] Lasse Hansen, Jasper Diesel, and Mattias P Heinrich. Multi-kernel diffusion cnns for graph-based learning on point clouds.

- In *Proceedings of the European Conference on Computer Vision (ECCV)*, pages 0–0, 2018. 2, 3
- [30] Kaiming He, Xiangyu Zhang, Shaoqing Ren, and Jian Sun. Deep residual learning for image recognition. In *Proceedings of the IEEE conference on computer vision and pattern recognition*, pages 770–778, 2016. 5
- [31] Wenchong He, Zhe Jiang, Chengming Zhang, and Arpan Man Sainju. Curvanet: Geometric deep learning based on directional curvature for 3d shape analysis. In *Proceedings of the 26th ACM SIGKDD International Conference on Knowledge Discovery & Data Mining*, pages 2214–2224, 2020. 2
- [32] Qingyong Hu, Bo Yang, Linhai Xie, Stefano Rosa, Yulan Guo, Zhihua Wang, Niki Trigoni, and Andrew Markham. RandLA-net: Efficient semantic segmentation of large-scale point clouds. In *2020 IEEE/CVF Conference on Computer Vision and Pattern Recognition (CVPR)*. IEEE, June 2020. 3
- [33] Evangelos Kalogerakis, Melinos Averkiou, Subhransu Maji, and Siddhartha Chaudhuri. 3D shape segmentation with projective convolutional networks. In *Proc. CVPR*, 2017. 2
- [34] Roman Klokov and Victor Lempitsky. Escape from cells: Deep kd-networks for the recognition of 3d point cloud models. In *2017 IEEE International Conference on Computer Vision (ICCV)*, pages 863–872. IEEE, 2017. 2
- [35] Ilya Kostrikov, Zhongshi Jiang, Daniele Panozzo, Denis Zorin, and Joan Bruna. Surface networks. In *Proceedings of the IEEE Conference on Computer Vision and Pattern Recognition*, pages 2540–2548, 2018. 3, 7
- [36] Alon Lahav and Ayellet Tal. Meshwalker: Deep mesh understanding by random walks. *arXiv preprint arXiv:2006.05353*, 2020. 2
- [37] Richard B Lehoucq, Danny C Sorensen, and Chao Yang. *ARPACK users’ guide: solution of large-scale eigenvalue problems with implicitly restarted Arnoldi methods*. SIAM, 1998. 4, 6
- [38] Ron Levie, Federico Monti, Xavier Bresson, and Michael M Bronstein. Caylenets: Graph convolutional neural networks with complex rational spectral filters. *IEEE Transactions on Signal Processing*, 67(1):97–109, 2018. 3
- [39] Bruno Levy. Laplace-beltrami eigenfunctions towards an algorithm that “understands” geometry. In *IEEE International Conference on Shape Modeling and Applications 2006 (SMI’06)*, pages 13–13. IEEE, 2006. 3
- [40] Maosen Li, Siheng Chen, Ya Zhang, and Ivor W. Tsang. Graph cross networks with vertex infomax pooling, 2020. 3
- [41] Qinsong Li, Shengjun Liu, Ling Hu, and Xinru Liu. Shape correspondence using anisotropic chebyshev spectral cnns. In *Proceedings of the IEEE/CVF Conference on Computer Vision and Pattern Recognition*, pages 14658–14667, 2020. 1, 3, 7, 8
- [42] Xianzhi Li, Ruihui Li, Guangyong Chen, Chi-Wing Fu, Daniel Cohen-Or, and Pheng-Ann Heng. A rotation-invariant framework for deep point cloud analysis. *arXiv preprint arXiv:2003.07238*, 2020. 2
- [43] Yangyan Li, Rui Bu, Mingchao Sun, and Baoquan Chen. Pointcnn. *arXiv preprint arXiv:1801.07791*, 2018. 2
- [44] Z Lian, A Godil, B Bustos, M Daoudi, J Hermans, S Kawamura, Y Kurita, G Lavoua, and P Dp Suetens. Shape retrieval on non-rigid 3d watertight meshes. In *Eurographics workshop on 3d object retrieval (3DOR)*, 2011. 6
- [45] Jian Liang and Hongkai Zhao. Solving partial differential equations on point clouds. *SIAM Journal on Scientific Computing*, 35(3):A1461–A1486, 2013. 2
- [46] Isaak Lim, Alexander Dielen, Marcel Campen, and Leif Kobbelt. A simple approach to intrinsic correspondence learning on unstructured 3d meshes. In *Proceedings of the European Conference on Computer Vision (ECCV)*, pages 0–0, 2018. 2
- [47] Zhi-Hao Lin, Sheng-Yu Huang, and Yu-Chiang Frank Wang. Convolution in the cloud: Learning deformable kernels in 3d graph convolution networks for point cloud analysis. In *Proceedings of the IEEE/CVF Conference on Computer Vision and Pattern Recognition (CVPR)*, June 2020. 3
- [48] Or Litany, Tal Remez, Emanuele Rodola, Alex Bronstein, and Michael Bronstein. Deep functional maps: Structured prediction for dense shape correspondence. In *Proceedings of the IEEE International Conference on Computer Vision*, pages 5659–5667, 2017. 3, 7
- [49] Zheng Ma, Junyu Xuan, Yu Guang Wang, Ming Li, and Pietro Lio. Path integral based convolution and pooling for graph neural networks, 2020. 3
- [50] Richard MacNeal. *The Solution of Partial Differential Equations by Means of Electrical Networks*. PhD thesis, Caltech, 1949. 3
- [51] Haggai Maron, Meirav Galun, Noam Aigerman, Miri Trope, Nadav Dym, Ersin Yumer, Vladimir G Kim, and Yaron Lipman. Convolutional neural networks on surfaces via seamless toric covers. *ACM Trans. Graph.*, 36(4):71–1, 2017. 6, 7, 8
- [52] Jonathan Masci, Davide Boscaini, Michael Bronstein, and Pierre Vandergheynst. Geodesic convolutional neural networks on riemannian manifolds. In *Proceedings of the IEEE international conference on computer vision workshops*, pages 37–45, 2015. 1, 2
- [53] Daniel Maturana and Sebastian Scherer. Voxnet: A 3d convolutional neural network for real-time object recognition. In *Intelligent Robots and Systems (IROS), 2015 IEEE/RSJ International Conference on*, pages 922–928. IEEE, 2015. 2
- [54] Mark Meyer, Mathieu Desbrun, Peter Schröder, and Alan H Barr. Discrete differential-geometry operators for triangulated 2-manifolds. In *Visualization and mathematics III*, pages 35–57. Springer, 2003. 1
- [55] Francesco Milano, Antonio Loquercio, Antoni Rosinol, Davide Scaramuzza, and Luca Carlone. Primal-dual mesh convolutional neural networks, 2020. 3
- [56] Federico Monti, Davide Boscaini, Jonathan Masci, Emanuele Rodola, Jan Svoboda, and Michael M Bronstein. Geometric deep learning on graphs and manifolds using mixture model cnns. In *Proceedings of the IEEE Conference on Computer Vision and Pattern Recognition*, pages 5115–5124, 2017. 2
- [57] Sayan Mukherjee and Qiang Wu. Estimation of gradients and coordinate covariation in classification. *Journal of Machine Learning Research*, 7(Nov):2481–2514, 2006. 4
- [58] Maks Ovsjanikov, Mirela Ben-Chen, Justin Solomon, Adrian Butscher, and Leonidas Guibas. Functional maps: a flexible representation of maps between shapes. *ACM Transactions on Graphics (TOG)*, 31(4):1–11, 2012. 3, 7

- [59] Adam Paszke, Sam Gross, Francisco Massa, Adam Lerer, James Bradbury, Gregory Chanan, Trevor Killeen, Zeming Lin, Natalia Gimelshein, Luca Antiga, et al. Pytorch: An imperative style, high-performance deep learning library. In *Advances in neural information processing systems*, pages 8026–8037, 2019. 6
- [60] Yifan Peng, Lin Lin, Lexing Ying, and Leonardo Zepeda-Núñez. Efficient long-range convolutions for point clouds. *arXiv preprint arXiv:2010.05295*, 2020. 2
- [61] Ulrich Pinkall and Konrad Polthier. Computing Discrete Minimal Surfaces and their Conjugates. *Exp. Math.*, 2(1), 1993. 3
- [62] Adrien Poulenard and Maks Ovsjanikov. Multi-directional geodesic neural networks via equivariant convolution. *ACM Transactions on Graphics (TOG)*, 37(6):1–14, 2018. 1, 2, 7, 8
- [63] Adrien Poulenard, Marie-Julie Rakotosaona, Yann Ponty, and Maks Ovsjanikov. Effective rotation-invariant point cnn with spherical harmonics kernels. In *2019 International Conference on 3D Vision (3DV)*, pages 47–56. IEEE, 2019. 2, 7
- [64] Charles R Qi, Hao Su, Kaichun Mo, and Leonidas J Guibas. Pointnet: Deep learning on point sets for 3d classification and segmentation. *Proc. Computer Vision and Pattern Recognition (CVPR), IEEE*, 1(2):4, 2017. 1, 2, 7
- [65] Charles Ruizhongtai Qi, Li Yi, Hao Su, and Leonidas J Guibas. Pointnet++: Deep hierarchical feature learning on point sets in a metric space. In *Advances in Neural Information Processing Systems*, pages 5105–5114, 2017. 2
- [66] Jing Ren, Adrien Poulenard, Peter Wonka, and Maks Ovsjanikov. Continuous and orientation-preserving correspondences via functional maps. *ACM Transactions on Graphics (TOG)*, 37(6):1–16, 2018. 7
- [67] Jean-Michel Roufosse, Abhishek Sharma, and Maks Ovsjanikov. Unsupervised deep learning for structured shape matching. In *Proceedings of the IEEE international conference on computer vision*, pages 1617–1627, 2019. 3
- [68] Raif M Rustamov. Laplace-beltrami eigenfunctions for deformation invariant shape representation. In *Proceedings of the fifth Eurographics symposium on Geometry processing*, pages 225–233, 2007. 3
- [69] Konstantinos Sfikas, Theoharis Theoharis, and Ioannis Pratikakis. Exploiting the panorama representation for convolutional neural network classification and retrieval. In *Eurographics Workshop on 3D Object Retrieval*, 2017. 2
- [70] Abhishek Sharma and Maks Ovsjanikov. Weakly supervised deep functional maps for shape matching. *Advances in Neural Information Processing Systems*, 33, 2020. 15
- [71] Nicholas Sharp and Keenan Crane. A laplacian for non-manifold triangle meshes. In *Computer Graphics Forum*, volume 39, pages 69–80. Wiley Online Library, 2020. 2, 3
- [72] Baoguang Shi, Song Bai, Zhichao Zhou, and Xiang Bai. Deeppano: Deep panoramic representation for 3-d shape recognition. *IEEE Signal Processing Letters*, 22(12):2339–2343, 2015. 2
- [73] Ayan Sinha, Jing Bai, and Karthik Ramani. Deep learning 3d shape surfaces using geometry images. In *European Conference on Computer Vision*, pages 223–240. Springer, 2016. 2
- [74] Hang Su, Subhransu Maji, Evangelos Kalogerakis, and Erik Learned-Miller. Multi-view convolutional neural networks for 3d shape recognition. In *Proceedings of the IEEE international conference on computer vision*, pages 945–953, 2015. 1, 2
- [75] Jian Sun, Maks Ovsjanikov, and Leonidas Guibas. A concise and provably informative multi-scale signature based on heat diffusion. In *Computer graphics forum*, volume 28, pages 1383–1392. Wiley Online Library, 2009. 5, 6
- [76] Zhiyu Sun, Ethan Rooke, Jerome Charton, Yusen He, Jia Lu, and Stephen Baek. Zernet: Convolutional neural networks on arbitrary surfaces via zernike local tangent space estimation. In *Computer Graphics Forum*. Wiley Online Library, 2020. 3
- [77] Hugues Thomas, Charles R Qi, Jean-Emmanuel Deschaud, Beatriz Marcotegui, François Goulette, and Leonidas J Guibas. Kpconv: Flexible and deformable convolution for point clouds. In *Proceedings of the IEEE International Conference on Computer Vision*, pages 6411–6420, 2019. 1, 2, 7, 15
- [78] Federico Tombari, Samuele Salti, and Luigi Di Stefano. Unique signatures of histograms for local surface description. In *European conference on computer vision*, pages 356–369. Springer, 2010. 5
- [79] Bruno Vallet and Bruno Lévy. Spectral geometry processing with manifold harmonics. In *Computer Graphics Forum*, volume 27, pages 251–260. Wiley Online Library, 2008. 3, 4
- [80] Nitika Verma, Edmond Boyer, and Jakob Verbeek. Feastnet: Feature-steered graph convolutions for 3d shape analysis. In *Proceedings of the IEEE conference on computer vision and pattern recognition*, pages 2598–2606, 2018. 2
- [81] Pauli Virtanen, Ralf Gommers, Travis E. Oliphant, Matt Haberland, Tyler Reddy, David Cournapeau, Evgeni Burovski, Pearu Peterson, Warren Weckesser, Jonathan Bright, Stéfan J. van der Walt, Matthew Brett, Joshua Wilson, K. Jarrod Millman, Nikolay Mayorov, Andrew R. J. Nelson, Eric Jones, Robert Kern, Eric Larson, C J Carey, İlhan Polat, Yu Feng, Eric W. Moore, Jake VanderPlas, Denis Laxalde, Josef Perktold, Robert Cimrman, Ian Henriksen, E. A. Quintero, Charles R. Harris, Anne M. Archibald, Antônio H. Ribeiro, Fabian Pedregosa, Paul van Mulbregt, and SciPy 1.0 Contributors. SciPy 1.0: Fundamental Algorithms for Scientific Computing in Python. *Nature Methods*, 17:261–272, 2020. 6
- [82] Daniel Vlastic, Ilya Baran, Wojciech Matusik, and Jovan Popović. Articulated mesh animation from multi-view silhouettes. In *ACM SIGGRAPH 2008 papers*, pages 1–9. 2008. 6
- [83] Peng-Shuai Wang, Yang Liu, Yu-Xiao Guo, Chun-Yu Sun, and Xin Tong. O-cnn: Octree-based convolutional neural networks for 3d shape analysis. *ACM Transactions on Graphics (TOG)*, 36(4):72, 2017. 2
- [84] Yue Wang, Yongbin Sun, Ziwei Liu, Sanjay E. Sarma, Michael M. Bronstein, and Justin M. Solomon. Dynamic graph cnn for learning on point clouds. *ACM Transactions on Graphics (TOG)*, 2019. 1, 2, 7
- [85] Lingyu Wei, Qixing Huang, Duygu Ceylan, Etienne Vouga, and Hao Li. Dense human body correspondences using convolutional networks. In *Computer Vision and Pattern Recognition*.

- niton (CVPR), 2016 IEEE Conference on, pages 1544–1553. IEEE, 2016. [2](#)
- [86] Ruben Wiersma, Elmar Eisemann, and Klaus Hildebrandt. Cnns on surfaces using rotation-equivariant features. *ACM Trans. Graph.*, 39(4), July 2020. [1](#), [2](#), [6](#), [7](#), [8](#), [15](#)
 - [87] Zhirong Wu, Shuran Song, Aditya Khosla, Fisher Yu, Linguang Zhang, Xiaoou Tang, and Jianxiong Xiao. 3d shapenets: A deep representation for volumetric shapes. In *Proceedings of the IEEE conference on computer vision and pattern recognition*, pages 1912–1920, 2015. [2](#)
 - [88] Kai Xu, Vladimir G Kim, Qixing Huang, Niloy Mitra, and Evangelos Kalogerakis. Data-driven shape analysis and processing. In *SIGGRAPH ASIA 2016 Courses*, page 4. ACM, 2016. [2](#)
 - [89] Li Yi, Hao Su, Xingwen Guo, and Leonidas J Guibas. Sync-speccnn: Synchronized spectral cnn for 3d shape segmentation. In *Proceedings of the IEEE Conference on Computer Vision and Pattern Recognition*, pages 2282–2290, 2017. [3](#)
 - [90] Hao Zhang, Oliver Van Kaick, and Ramsay Dyer. Spectral mesh processing. In *Computer graphics forum*, volume 29, pages 1865–1894. Wiley Online Library, 2010. [3](#), [4](#)
 - [91] Zhiyuan Zhang, Binh-Son Hua, David W Rosen, and Sai-Kit Yeung. Rotation invariant convolutions for 3d point clouds deep learning. In *2019 International Conference on 3D Vision (3DV)*, pages 204–213. IEEE, 2019. [2](#)
 - [92] Yongheng Zhao, Tolga Birdal, Jan Eric Lenssen, Emanuele Menegatti, Leonidas Guibas, and Federico Tombari. Quaternion equivariant capsule networks for 3d point clouds. *ECCV 2020*, 2020. [2](#)
 - [93] Yi Zhou, Chenglei Wu, Zimo Li, Chen Cao, Yuting Ye, Jason Saragih, Hao Li, and Yaser Sheikh. Fully convolutional mesh autoencoder using efficient spatially varying kernels, 2020. [3](#)

A. An Argument for Generality

In Sec. 3, we propose learned diffusion at various timescales followed by learned pointwise functions as the first two components of our method. Although this formulation clearly offers nonlocal support to the learned pointwise functions, it is not immediately clear how general the resulting function space is. In particular, it is significant to show that this function space includes at least radially symmetric convolutions, a most basic building block which has appear widely in past work. This treatment of radially symmetric convolutions arises because points on surfaces do not have canonical orientations (though it should be noted that recent work has since focused on expanding beyond symmetric filters, and our own method includes gradient features for precisely this purpose).

Lemma 1 of the main document states that, at least in the flat continuous setting, our construction is sufficiently general to represent radially symmetric convolutions. Here, we present the full version of this argument.

To begin, consider the convolution of a scalar field in the plane $x : \mathbb{R}^2 \rightarrow \mathbb{R}$ against a radially symmetric filter $\alpha(r) : \mathbb{R}_{\geq 0} \rightarrow \mathbb{R}$. Recall that the value of the convolution at p depends only on $X_p(r) := \int_{\theta \in [0, 2\pi)} x(p + r[\cos \theta, \sin \theta])$, the average of the field x along the boundary of a ball with radius r centered at p . In particular, we have

$$\begin{aligned} (x * \alpha)(p) &= \int_{q \in \mathbb{R}^2} x(q) \alpha(|p - q|) \\ &= \int_{r \in (0, \infty)} r \alpha(r) X_p(r) \end{aligned} \quad (6)$$

where the equality moves to polar coordinates. Thus for any convolution against a radial filter α , there exists a function σ which at each point p takes the function $X_p(r)$ as input and produces the value of the convolution against α at p .

We wish to argue that our pointwise functions can represent σ , but the obstacle is that these pointwise functions do not receive $X_p(r)$ as input; they instead receive $x_p(t)$, the values of x at p after diffusion for some times t . In the continuous limit, this is really the function $x_p(t)$ holding the diffused value of x at p for all times t . We will show that these diffused values are sufficiently informative to serve the same purpose. More precisely, we will argue that there must exist a function which maps $x_p(t)$ to $X_p(r)$.

Recall that the heat kernel in \mathbb{R}^2 is given by

$$K_t(r) := \frac{1}{4\pi t} e^{-\frac{r^2}{4t}} \quad (7)$$

and diffusion of the scalar field x for time t is then

$$\begin{aligned} x_p(t) &= \int_{q \in \mathbb{R}^2} K_t(|p - q|) x(q) \\ &= \int_{r \in (0, \infty)} r \int_{\theta \in [0, 2\pi)} K_t(r) x(p + r[\cos \theta, \sin \theta]) \\ &= \int_{r \in (0, \infty)} K_t(r) r X_p(r) \\ &= \frac{1}{4\pi t} \int_{r \in (0, \infty)} e^{-\frac{r^2}{4t}} r X_p(r). \end{aligned} \quad (8)$$

We next argue that this integral is “invertible”, that $X_p(r)$ can be recovered from $x_p(t)$, via an inverse Laplace transform. First, we introduce the reparameterizations $\bar{t} := 1/t$ and $\bar{r} := \frac{r^2}{4}$, yielding

$$x_p(\bar{t}) = \frac{\bar{t}}{2\pi} \int_{\bar{r} \in (0, \infty)} e^{-\bar{r}\bar{t}} X_p(2\sqrt{\bar{r}}). \quad (9)$$

This expression has the form a Laplace transform \mathcal{L} , as

$$x_p(\bar{t}) = \frac{\bar{t}}{2\pi} \mathcal{L}\{X_p(2\sqrt{\bar{r}})\}(\bar{t}). \quad (10)$$

The Laplace transform is invertible, as are the reparameterizations, implying the existence of an inverse function.

This completes our argument. There exists some function, which we will denote by γ , mapping $x_p(t)$ to $X_p(r)$ (in fact, γ has the form of an inverse Laplace transform). Composing γ with $\sigma \circ \gamma(x_p(t))$ implies that, for a radial filter $\alpha(r)$, there exists some pointwise function which takes as input $x_p(t)$ and evaluates the convolution against α at p .

Of course, this argument merely says that such a function exists in the flat, continuous setting. In practice we approximate pointwise functions via finite-dimensional MLPs, and merely evaluate diffusion at a collection of times t . Extending this argument from the continuous setting to a universal approximation proof in the discrete setting would require careful consideration of the relevant function spaces, which is beyond the scope of this work. Similarly, extending this argument from \mathbb{R}^2 to curved manifolds would require a deeper analysis, though the same essential properties hold for diffusion on surfaces. Nonetheless, we consider this construction to be important evidence that diffusion followed by pointwise functions is an expressive function space, supported by the strong results of our method in practical experiments.

B. Methods Discussion

B.1. Orientation

In Sec. 3.4 we describe a simple strategy for generating additional features from the spatial gradients of each scalar channel, expanding the space our operator beyond radially-symmetric filters. These features are learned using a $C \times C$

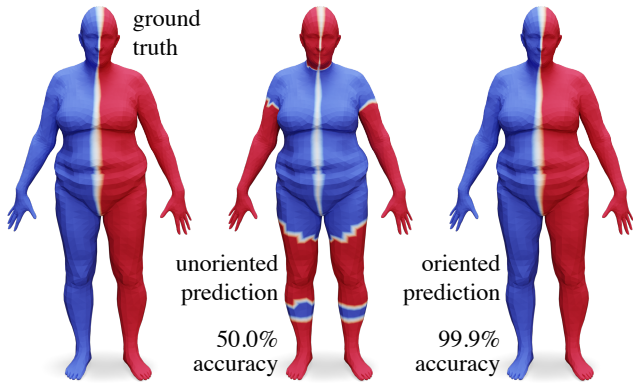


Figure 6. Our network naturally encodes a notation of orientation, allowing it to disambiguate bilateral symmetry even in a purely-intrinsic formulation (*right*). Substituting an unoriented term removes the effect (*middle*).

matrix A —choosing A to be a real matrix models a linear combination of tangent vectors, whereas choosing A to be complex models a more general linear combination of *rotated* tangent vectors. These rotations implicitly leverage a notion of consistent outward normal orientation for the surface, because rotating a tangent vector has the opposite effect when the normal orientation is inverted. Accordingly, on surfaces where no consistent normals are available such as raw point clouds, real A should be used. However, using complex A on an oriented surface allows the network to leverage the orientation structure. In particular, these learned rotations allow our method to disambiguate bilateral symmetry even in a purely intrinsic representation—a common challenge in shape correspondence.

We demonstrate this behavior via a simple artificial experiment in which we classify the left vs. right side of human models from the FAUST dataset [7] using a purely intrinsic 32-width DiffusionNet with HKS as input. On the original dataset, asymmetric biases—such as a template mesh with asymmetric connectivity—make it unintentionally easy to distinguish left from right. We cancel the effect of these biases by augmenting the dataset with a copy of each mesh that has been mirrored across the left-right axis (preserving orientation by inverting triangles). With a complex-valued A , our network is able to easily distinguish left from right with 99.9% accuracy, despite both a purely intrinsic architecture and intrinsic input features (Fig. 6). Simply restricting to real-valued A renders the network unable to disambiguate the symmetry, with a totally random 50.0% accuracy.

B.2. Subsampling

In order to gain additional robustness to changes in sampling density of the input shapes, we propose an augmentation strategy which uniquely leverages our formulation.

Ablation	Accuracy
no diffusion	84.1 %
fixed-time diffusion	85.0 %
no gradient features	83.1 %
unlearned gradient features	83.6 %
(full method)	90.9 %

Table 6. An ablation study, evaluated on the human segmentation task. Omitting any of the components of our method leads to a significant drop in performance. Manually fixing a non-optimal diffusion time ($t = 0.5$) renders diffusion largely useless—our learned procedure automatically optimizes a diffusion time for each channel.

Specifically, we randomly sub-sample the vertices of a mesh (or points in a point cloud) retaining some fraction $\rho \in [0, 1]$ of the vertices. However, we *do not* explicitly form a mesh (resp. point cloud) from these sampled vertices, and thus do not, e.g., recompute the Laplacian eigenbasis. Instead, we simply apply our pointwise MLPs only at a masked vertices, and mask out the corresponding entries of the eigenbasis—with these small changes our networks can be evaluated on the subsampled input without explicitly forming a simplified mesh. After subsampling, the eigenbasis will no longer be orthonormal; we then simply renormalize each eigenvector independently. Orthogonality could in-principle be also recovered via Gram-Schmidt orthogonalization, but we do not find this necessary in practice as the subsampled eigenbases are nearly orthogonal. If necessary to evaluate a loss, the outputs of our network on the sampled vertices can be projected through the eigenbasis to the original vertices.

All of these operations are straightforward linear algebra, yielding a simple computational scheme for subsampled evaluation, which can easily be used for augmentation at training time. We do not find this procedure necessary in our experiments, but it may be an important tool *e.g.* when learning mesh-agnostic functions on very small datasets.

C. Analysis

Ablation To validate the components of our approach, we present a simple ablation study on the human segmentation task from Sec. 5.2, using raw coordinates as input. Results are presented in Tab. 6. The variant *no diffusion* omits the diffusion layer from each DiffusionNet block, *fixed-time diffusion* manually specifies a diffusion time, *no gradient features* omits the gradient features, and *unlearned gradient features* includes gradient features but omits the learned transformation of gradient vectors A . We observe a noticeable drop in accuracy when omitting any of the components of the method. Manually specifying a non-optimal diffusion time ($t = 0.5$) yields a network with significantly worse accuracy compared to our learned approach. A key advantage of learned diffusion is that this time is automatically tuned

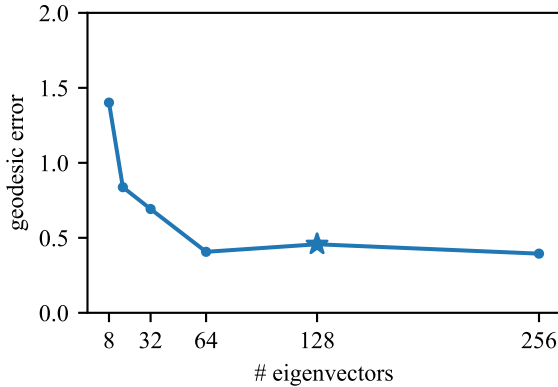


Figure 7. The effect of varying the size of the truncated spectral basis in our method, evaluated on FAUST vertex-labelling correspondence. Errors are measured in mean geodesic distance $\times 100$, after normalizing by the geodesic diameter. We use 128 eigenvectors in all experiments (marked by the star).

by the optimization process, individually for each feature channel.

Spectral basis size Our method evaluates diffusion using a truncated spectral basis (Sec. 3.3); the larger the size of the basis, the more accurately diffusion is resolved. In Fig. 7 we vary the size of this truncated basis for the FAUST vertex-labelling correspondence task as in Tab. 5, measuring accuracy on the original test set. We find performance degrades significantly with fewer than 64 eigenvectors on this problem, whereas using more than 128 offers negligible benefit—our experiments use $k = 128$ eigenvectors as a safe default.

D. Extended Results

Here we provide additional result tables and plots for the experiments from Sec. 5.

Functional correspondence In Sec. 5.3 we evaluate our method in the context of shape correspondence via functional maps, using DiffusionNet as a learned feature extractor. In Tab. 7 we provide additional quantitative results on an aligned variant of the dataset [70], using coordinates as input without random rotation augmentations. As before, DiffusionNet outperforms other recent approaches as a feature extractor, particularly when training on one dataset and testing on another.

Additionally, in Fig. 8 we visualize qualitative results from the unaligned correspondences as reported in Tab. 4 by transferring textures through the resulting maps. Here, all methods yield a plausible solution when trained on the same dataset as the query pair (SCAPE), but only DiffusionNet yields good results after training on a different dataset

Method / Dataset	FAUST	SCAPE	FonS	SonF
KPConv - xyz [77]	2.87	5.32	5.23	3.20
HSN - xyz [86]	3.28	3.41	7.50	3.79
DiffusionNet - xyz (ours)	2.56	3.04	4.19	2.79

Table 7. Additional results from feature learning for functional shape correspondence. Here, training and testing shapes face the same direction, and methods are trained without random rotation augmentation. Values are mean geodesic error $\times 100$, after normalizing shapes to have area 1.

(FAUST).

Sampling invariance In Fig. 9 show geodesic error plots for the vertex-labelling correspondence problem, which we use to study the invariance of our method with respect to remeshing and resampling operations (Sec. 5.4), as reported in Tab. 5. Only our method maintains an accurate solution when applied to remeshed variants of the test shapes. Furthermore, the trained DiffusionNet can even be applied directly to a sampled point cloud, while still yielding similar results.

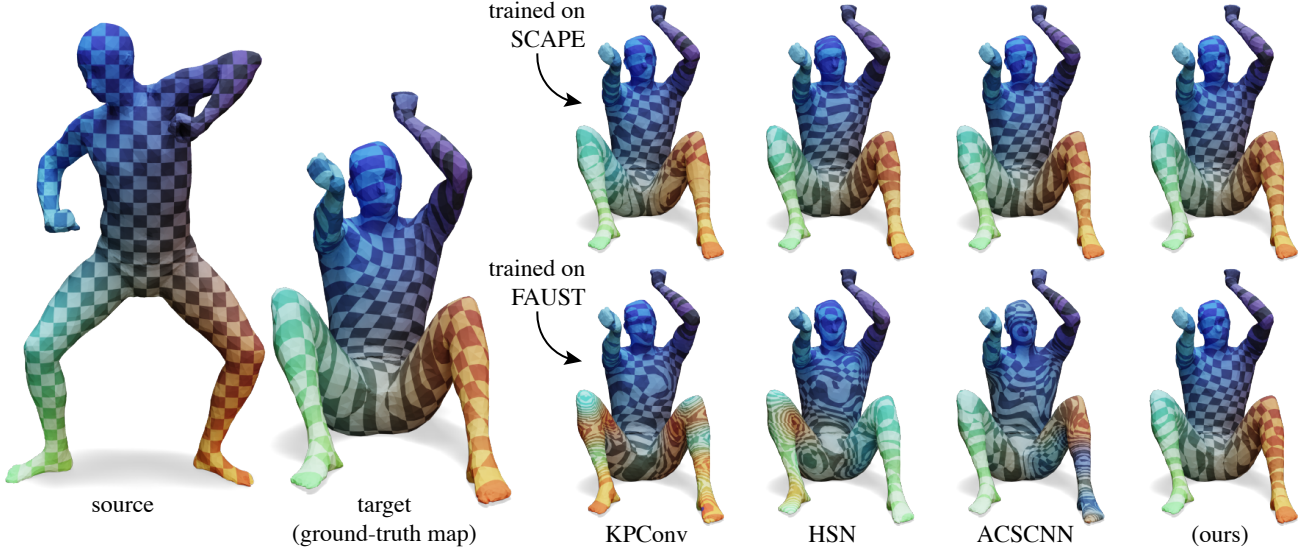


Figure 8. Functional map correspondences from Sec. 5.3, visualized by transferring a texture through the map for a challenging test pair. All methods yield visually a plausible solution when trained on the same dataset as the query pair (SCAPE, *top row*), but only DiffusionNet yields good results after training on a different dataset (FAUST, *bottom row*).

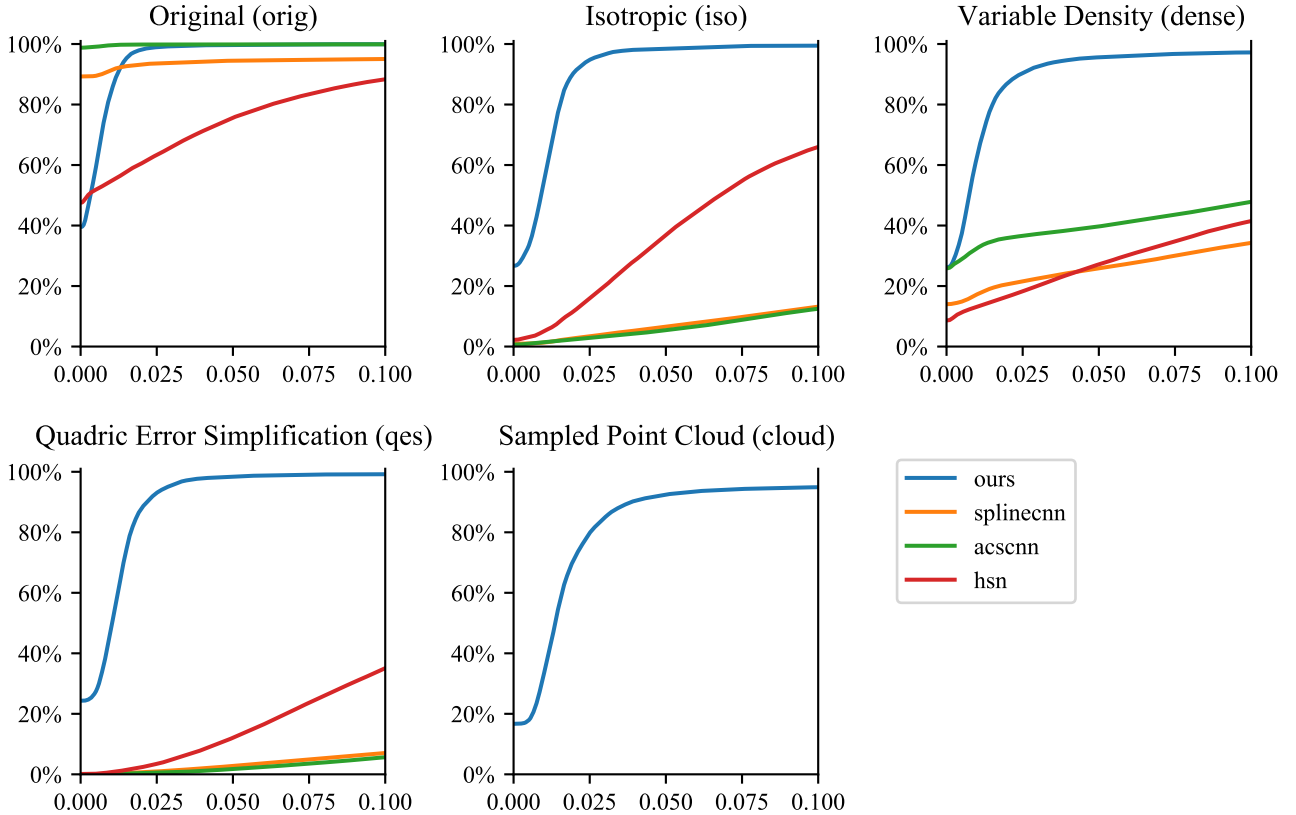


Figure 9. Accuracy curves for vertex-labelling correspondence on the FAUST dataset, as in Tab. 5; only DiffusionNet retains its accuracy as the shapes are remeshed (or even sampled to a point cloud). The first plot gives accuracy on the original test meshes, and the subsequent plots denote testing on remeshed variants of the test set. Only DiffusionNet can be directly applied to the sampled point cloud. For each plot, the x-axis is the geodesic error (normalized by geodesic diameter), and the y-axis is the percent of vertex correspondences within that error.